JACS
JOURNAL OF THE AMERICAN CHEMICAL SOCIETY

Article

Enzyme-Like Click Catalysis by a Copper-Containing Single-Chain Nanoparticle

Junfeng Chen, Jiang Wang, Yugang Bai, Ke Li, Edzna S. Garcia, Andrew L. Ferguson, and Steven Zimmerman

J. Am. Chem. Soc., **Just Accepted Manuscript** • DOI: 10.1021/jacs.8b06875 • Publication Date (Web): 07 Sep 2018

ACS Publications

is published by the American Chemical Society. 1155 Sixteenth Street N.W., Washington, DC 20036

Enzyme-Like Click Catalysis by a Copper-Containing Single-Chain Nanoparticle

Junfeng Chen,[†] Jiang Wang,[‡] Yugang Bai,[†] Ke Li,[†] Edzna S. Garcia,[†] Andrew L. Ferguson,[§] and Steven C. Zimmerman*[,†]

[†]Department of Chemistry, University of Illinois at Urbana−Champaign, Urbana, Illinois 61801, United States
[‡]Department of Physics, University of Illinois at Urbana−Champaign, Urbana, Illinois 61801, United States
[§]Institute for Molecular Engineering, 5640 South Ellis Avenue, Chicago, Illinois 60637, United States

Supporting Information

ABSTRACT: A major challenge in performing reactions in biological systems is the requirement for low substrate concentrations, often in the micromolar range. We report that copper crosslinked single-chain polymeric nanoparticles (SCNPs) are able to significantly increase the efficiency of copper(I)-catalyzed alkyne-azide cycloaddition (CuAAC) reactions at low substrate concentration in aqueous buffer by promoting substrate binding. Using a fluorogenic click reaction and dye uptake experiments, a structure-activity study is performed with SCNPs of different size and copper content and substrates of varying charge and hydrophobicity. The high catalytic efficiency and selectivity is attributed to a mechanism that involves an enzyme-like binding process. Saturation transfer difference (STD) NMR spectroscopy, 2D-NOESY NMR, kinetic analyses with varying substrate concentration, and computational simulations are consistent with a Michaelis-Menten, two-substrate random sequential enzyme-like kinetic profile. This general approach may prove useful for developing more sustainable catalysts and as agents for biomedicine and chemical biology.

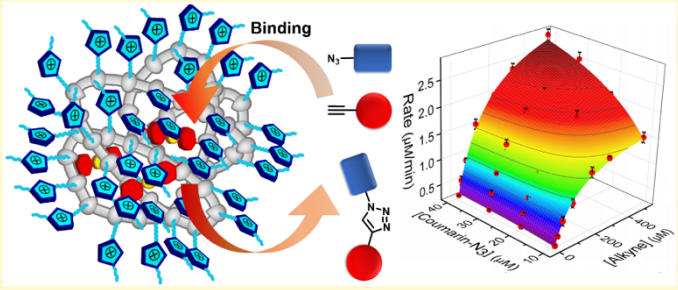

INTRODUCTION

Metalloenzymes often achieve their remarkable catalytic efficiency and selectivity through an architecture that places a substrate binding site in close proximity to a reactive metal center. The result is an enzymatic reaction that is fast, clean, and selective despite the complex and competitive aqueous bioenvironment. The protein scaffold plays a key role in protecting the reactive metal center. Not surprisingly, considerable effort has focused on developing artificial metalloenzymes.[1] In parallel, an increasing number of transition metal catalysts have been developed that function in aqueous media, some sufficiently biocompatible to operate inside the competitive environment of living cells.[2] These advances have exciting implications for sustainable chemistry and as powerful new tools for chemical biology and medicinal chemistry.[2d] Nonetheless, significant hurdles remain especially in living systems where the required low substrate concentration and physiological pH and temperature often results in low reaction rates. The further demands for low toxicity and compatibility with a broad range of redox-active and coordinating functionality suggests that improvements in catalytic efficiency and biocompatibility may require a protein-like shell for shielding the metal center and for substrate binding.

Recently, there has been intense interest in metal-containing, catalytic, single-chain nanoparticles (SCNPs) formed by intramolecular crosslinking.[3] The cross-linked polymers loosely resemble the folded polypeptide structure of bioactive enzymes. More importantly, the wide array of polymerization methods and cross-linking chemistries available to produce SCNPs opens the door to a remarkably broad range of structures and structural tunability. To date, water-soluble, catalytic SCNPs have been reported for copper(I)-catalyzed alkyne-azide cycloaddition (CuAAC),[4] enantio- and diastereo-selective aldol reaction,[5] ketone reduction,[6] palladium-mediated depropargylation,[7] enantio-selective sulfur oxidation[8] and phenol hydroxylation[9] reactions as well as for living radical polymerization processes.[10] As impressive as these examples are, there have been very limited demonstrations of enzyme-like kinetics[11] and only few explorations of the putative hydrophobic binding sites, for example, through structure-activity relationships.[12]

Our interest in cross-linked polymers as organic nanoparticles[13] and their host-guest capabilities[14] has led us to study their cell uptake[15] and the possibility of creating selective, nanoscale intracellular catalysts.[3] We recently reported a single-chain metal-organic nanoparticle, cross-linked by copper coordination chemistry that effected the well-known CuAAC click reaction[16] at ppm levels of copper, both in water and in mammalian and bacterial cells.[4] Herein, we report the synthesis of SCNPs with different structures that has allowed us to develop a structure-activity relationship as well as to shed light on the overall reaction mechanism. The copper containing SCNPs show enzyme-like behavior, in particular substrate binding that increases the reaction rate and selectivity. The results suggest that the high catalytic efficiency of SCNPs may be attributed to their enzyme-like structure. As the first demonstration of dual saturation kinetics, this approach to metallo-enzyme-mimicry that combines metal centers and a polymeric scaffold should provide a useful strategy for future catalyst design and development.

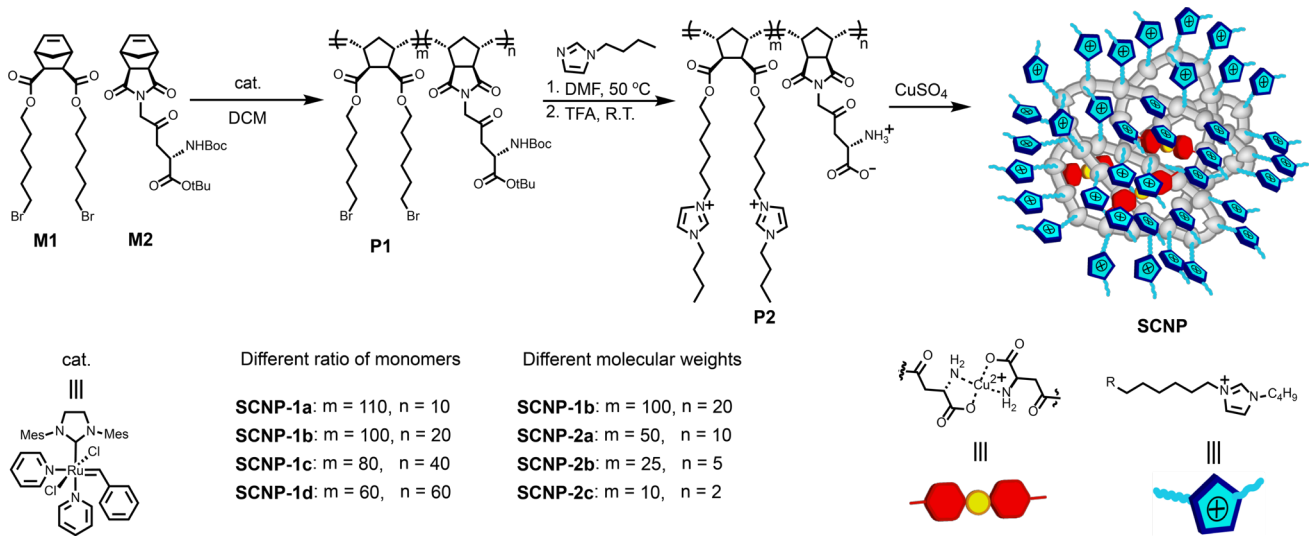

Figure 1. Illustration of the synthesis of the copper crosslinked single-chain organic nanoparticles (SCNPs)

EXPERIMENTAL SECTION

Materials and Instrumentation. Details regarding the chemical reagents used, synthetic procedures for polymers and substrates used in reactions with SCNP catalysts, instrumentation used in this work, and additional details on the computational methods can be found in the Supporting Information.

Procedure for Fluorogenic Click Reactions and Kinetic Analysis. The CuAAC click reaction was monitored using fluorescence-quenched coumarin azide **1** and alkyne **2**.[17] After the click reaction, **1** forms compound **3** with restored fluorescence (Scheme 1). In a 0.7 mL fluorimeter cuvette, SCNPs, sodium ascorbate and a DMSO solution of substrate was added in 0.5 mL PBS buffer at pH = 7.4. The ascorbic acid concentration was 2 mM and the final amount of DMSO was 2% (v/v). The intensity was monitored by fluorimeter every 10 s at λ_{em} = 488 nm with λ_{ex} = 410 nm. The reaction conversion was calculated from the observed fluorescence intensity using pure **3** as the standard. Relative rates were determined as follows. Approximately 1 min after initiating the reaction the increase in fluorescence stabilized and became linear over time. The slope of the fluorescence vs time plot starting at ca. 2 min and using 10-15 data points collected every 10 s was used for the calculation of relative rates.

For kinetic studies, a 4 μM aqueous solution of **SCNP-2a** was used. The concentration of **1** was varied from 10 μM to 40 μM, whereas the concentration of **2** was varied from 12.5 μM to 500 μM due to its higher water solubility. The collected kinetic data was fit to various models but a random sequential two-substrates enzyme kinetics equation gave the best fit.[18]

Scheme 1

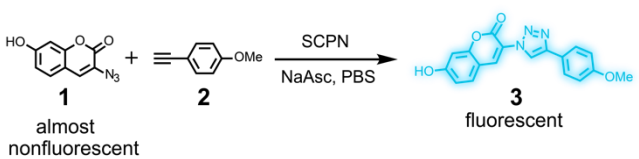

Pyrene Uptake Experiments. The uptake of pyrene as a hydrophobic guest by SCNPs was quantified by shaking a vial containing 0.2 mL of a 1 M pyrene solution in chloroform with 1 mL of a 5 μM aqueous solution of **SCNP-1b** (or the weight equivalent of other SCNPs).[19] The vial underwent centrifugation and the aqueous layer removed using a syringe. A UV-vis spectrophotometer was used to measure the absorbance of pyrene in the aqueous layer, a direct measure of the amount solubilized by the SCNP.

STD NMR Method. SCNP-2a was dissolved in D_2O at a concentration of 100 μM, and the substrate was added as a 200 mM DMSO-d_6 solution to reach a final concentration of 2 mM (20 equivalents). Spectra were collected after selectively irradiating **SCNP-2a** to saturation at δ 1.2 ppm a spectral region where there were no substrate signals. During the saturation period, the magnetization was transferred through intra/intermolecular spin diffusion to other protons on the SCNP as well as to the bound substrates, which further transferred to free molecules due to the exchange of free and bound substrates.

Molecular Dynamics Simulation of SCNP-Substrate Binding. All the SCNP-2a simulations were conducted using the GROMACS 4.6 simulation suite.[20] The binding process was studied with different substrates. The linear polymers were first crosslinked by connecting the copper ions and amino acid groups, and then placed in a 11 nm cubic box of water molecules. The system was simulated at 300 K and 1 bar for 100 ns at which time the SCNP had folded into a stable globular structure. Subsequently 20 copies of one specific substrate molecule were randomly placed into the box and the simulation continued for 20 ns. After discarding the first 10 ns for equilibration, substrate binding was quantified by counting the number of substrate molecules within the nanoparticle over the course of the terminal 10 ns.

RESULT AND DISCUSSION

Synthesis and Characterization of SCNPs. Using a modified procedure based on our original report,[4] **P1** were prepared by ring-opening metathesis polymerization (ROMP) of monomers **M1** and **M2** with pyridine-modified Grubbs third-generation catalyst (Figure 1).[21] Monomer content and degrees of polymerization (DPs) were controlled by adjusting the feed ratios of monomers and the amount of Grubbs catalyst during the ROMP.

Formation of **P1** was confirmed by gel-permeation chromatography (GPC), which showed a good correlation between the measured molecular weights and the catalyst and monomer feed ratios, as well as low polydispersity indices (PDI) that ranged from 1.01 to 1.05. The **P1** were post-functionalized by treatment with *N*-butyl-imidazole providing imidazolium groups that afforded water-soluble, amphiphilic

polymers. Finally, the amino acid residues were deprotected with trifluoroacetic acid (TFA). The resulting **P2** were purified by precipitation in ether followed by dialysis against water. The post-functionalized polymers **P2** were characterized by NMR spectroscopy.

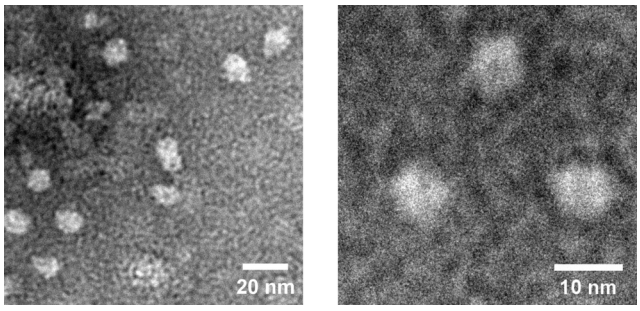

Figure 2. TEM images of **SCNP-2a**.

Given that several α-amino acids are reported to form stable complexes with Cu(II) and Cu(I) with 2:1 stoichiometries,[22] 0.5 eq of $CuSO_4$ relative to the aspartate units was added to **P2** to form Cu(II)-containing SCNP. The resulting nanoparticles were characterized by transmission electron microscopy (TEM) (Figure 2) and dynamic light scattering (DLS, Figure S10). For the representative **SCNP-2a**, the TEM-determined diameter was ca. 8-10 nm, which was larger than the 5.8 nm size determined by DLS. Despite cross-linking, the polymeric nanoparticles can flatten when absorbed on the grid surface[13c] and the ammonium molybdate negative staining further increases the observed diameter. The DLS-measured hydrodynamic size of 5.8 nm is quite reasonable for a 37 kDa polymeric nanoparticle and close to the computationally determined diameter of 5-6 nm (vide infra). Overall, the data are consistent with a SCNP. Because of their greater stability, SCNPs were kept in aqueous solution as Cu(II) complexes. For performing CuAAC click reactions, sodium ascorbate was added to produce the Cu(I) SCNPs in situ.

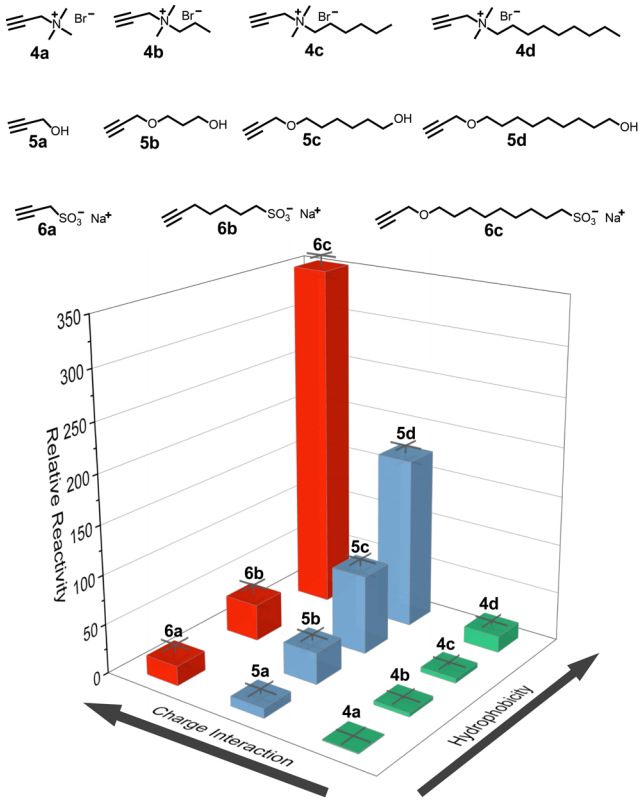

Figure 3. Structures of substrates with hydrophobicity and charge. Fluorogenic reaction rate of different substrates with of **SCNP-2a** (4 μM), **1** (20 μM), **4-6** (40 μM) and sodium ascorbate (2 mM) in PBS buffer pH = 7.4. Rates are relative to that of **4a**. Error bars are standard deviations of three independent runs.

Rate of CuAAC Reactions and Substrate Selectivity. To test whether substrate charge or hydrophobicity affect the SCNP-catalyzed fluorogenic click reaction, alkyne substrates **4-6** were prepared and mixed with azide **2**, **SCNP-2a**, and ascorbic acid. For comparison, the reactivity of the same substrates was examined using the most highly active tris(triazolylmethyl)amine-based ligand for Cu(I) developed by Liu, Marlowe, Wu, and coworkers known as BTTAA[23] (see Figure S11). In general, **4-6** show only small (<2-fold) rate differences with BTTAA. In contrast, with **SCNP-2a**, along each homologous series of substrates, **4a**-**4d**, **5a**-**5d**, and **6a**-**6c**, the rate of click reaction increased dramatically with increasing length of the aliphatic chain indicating the importance of substrate hydrophobicity (Figure 3). Substrates **4d**, **5d** and **6c** with the longest aliphatic chains were on average 25 times faster than substrates **4a**, **5a** and **6a** with the shortest chains. The importance of hydrophobic binding by the SCNP is further illustrated by the 6-fold rate increase for **6a** seen with **SCNP-2a** relative to BTTAA despite the amino acid-Cu(I) complex being a comparatively poor catalyst.

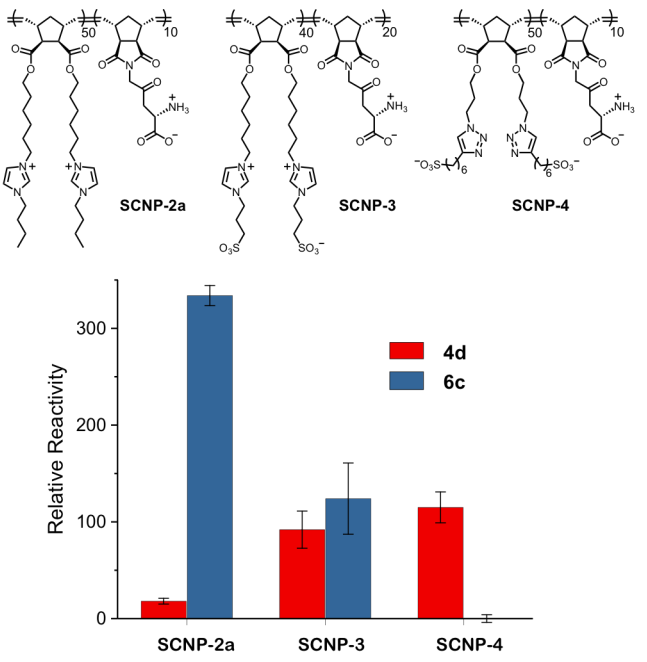

Figure 4. Structure of cationic, zwitterionic, and anionic **SCNPs 2a**, **3**, and **4**, respectively and relative reaction rates of substrates **4d** and **6c** in the fluorogenic click reaction. Conditions were **SCNP** (4 μM), **1** (20 μM), **4d** and **6c** (40 μM) and sodium ascorbate (2 mM) in PBS buffer pH = 7.4. Rates are relative to that of **SCNP-4** with **4d**. Error bars are standard deviations of three

The other trend evident in the Figure 3 data is that charge significantly influences substrate reactivity. Thus, the click reaction of negatively charged substrate **6c** is two times faster than neutral substrate **5d**, and 20 times faster than cationic substrate **4d**. With BTTAA there is a small advantage for the cationic alkynes **4**, but the largest rate difference (**4a** vs. **6a**) is three-fold and as indicated above, most rates are <2-fold different. The structure activity relationship that emerges from Figure 3 is that polycationic **SCNP-2a** selectively takes up hydrophobic substrates with a preference for anionic over neutral guests whereas an electrostatic repulsion significantly disfavors cationic substrates.

To further study the effect of charge and broaden the substrate selectivity, two additional SCNPs (**SCNP-3** and **SCNP-4**) were prepared (see Figure 4 and Supporting Information). Thus, zwitterionic

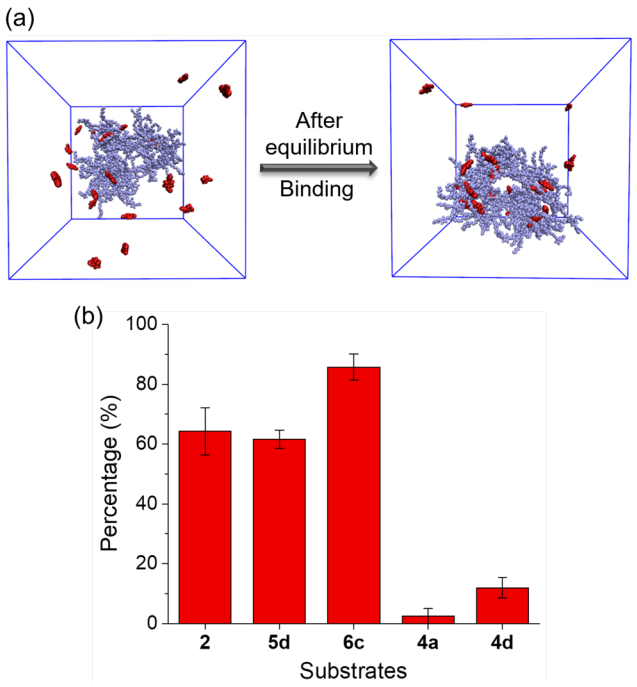

Figure 5. (a) Snapshot of **SCNP-2a** and **2** in an 11 Å water box (water not shown) before and after equilibrium. Polymer atoms were colored as blue, substrate molecule were colored red and solvent molecules were turned off. (b) Percentage of substrate molecules within the nanoparticle averaged over the terminal 10 ns of the simulation. Error bars represent standard deviations of the percentage measured over the equilibrium portion.

SCNP-3 and anionic **SCNP-4** were designed to test whether the substrate preference in Figure 3 could be altered. Their catalytic performance in the fluorogenic CuAAC reaction was tested with cationic alkyne **4d** and anionic alkyne **6c** and compared to that with **SCNP-2a**. As shown in Figure 4, **SCNP-4** processed cationic alkyne **4d** significantly faster than did **SCNP-2a** whereas almost no reaction was measured with **6c** which reversed the selectivity profile of **SCNP-2a**. On the other hand, the zwitterionic **SCNP-3** exhibited similar rates towards both cationic and anionic substrates.

The SCNP is critical for the catalysis observed. Thus, BTTAA was used to test the role of the polymer in the control experiments (Figure S11) because no reaction could be observed with the copper complex of glycine. The data presented in Figures 3 and 4 suggest clearly that one key role played by the polymeric nanoparticle is in binding the substrates in proximity to the metal catalyst. To obtain more than inferential support for the substrate binding model, we examined the binding both computationally and experimentally.

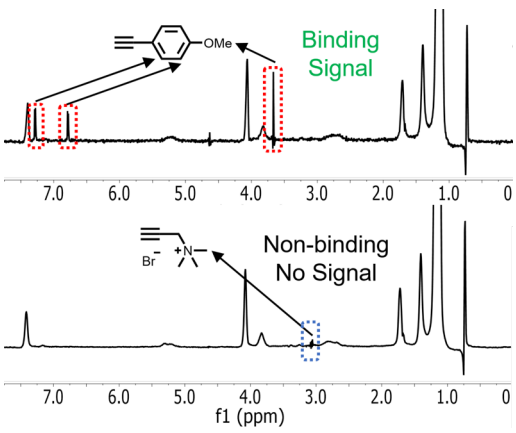

Figure 6. STD spectrums for **SCNP-2a** (100 μM) with **2** (2 mM) or **4a** (2mM) in D_2O.

Molecular Dynamics Simulation of Substrate Binding Within SCNP. The potential binding process was studied by molecular dynamics simulation (see Experimental Section and Supporting Information for additional details). When the **SCNP-2a** structure was built and modeled computationally, it was found to adopt a globular shape with a diameter of ca. 5-6 nm. The substrate-nanoparticle interaction was evaluated by calculating the percentage of small molecules that reside inside the nanoparticle. As shown in Figure 5 and Supporting Movie 1, coumarin azide **2** is mostly bound and differential substrate uptake was observed for **4a**, **4d**, **5d**, and **6c** that is consistent with the dependence on the hydrophobicity and charge seen experimentally in Figure 3.

Substrate Binding is Detected by NMR. To obtain direct experimental evidence of substrate binding, saturation transfer difference (STD) spectroscopy was applied to **SCNP-2a** and alkynes **2** and **4a** to observe possible nuclear Overhauser effect (NOE) between catalyst and substrate. STD has been commonly used to study the interaction between proteins and guest ligands.[24] STD spectra were measured separately for 20 equivalents of **2** and **4a** mixed with **SCNP-2a**. As shown in Figure 6, the hydrophobic substrate **2** exhibited relatively strong signals indicating residence within the polymeric nanoparticle. In contrast, the positively charged and hydrophilic substrate **4a** showed negligible signal. These results support substrate binding and are consistent with the observed reaction kinetics.

The binding between substrate **2** and **SCNP-2a** was further elucidated by two-dimensional nuclear Overhauser effect spectroscopy (2D-NOESY). As seen in Figure 7, substrate **2** gives signals at δ 7.3, 6.8, and 3.7 ppm all three of which exhibit strong cross-peaks to SCNP peaks appearing between δ 0.5 - 2.0 ppm. This region contains the signals of hydrophobic aliphatic chains. In contrast, the alkene region from the polymer backbone showed almost no NOE signal although it is also hydrophobic. These results suggest that hydrophobic substrates may preferentially bind within pockets formed by the aliphatic side-chains and the imidazolium groups.

Probing the Importance of the SCNP MW, Copper Content, and Amphiphilic Structure. If hydrophobic binding by the amphiphilic side-chains of the SCNP is important to the catalysis then changing the ratio of the aliphatic to imidazolium content within the side-chains would be expected to alter the rate of the click reaction. Thus, **SCNP-5** and **SCNP-**

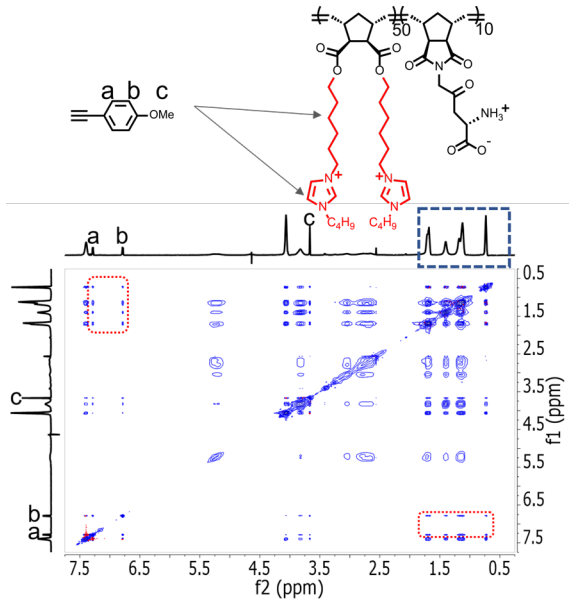

Figure 7. 2D-NOESY spectrum of SCNP-**2a** (100 μM) with **2** (2 mM) in D_2O.

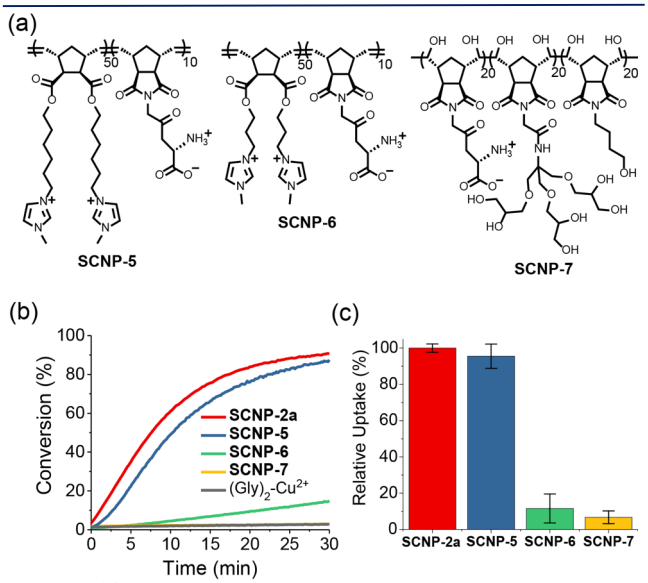

Figure 8. (a) Polymer parent structures of SCNPs with different water solubilization structure. (b) Reaction kinetics of SCNPs with SCNPs (4 μM), **1** (20 μM), **2** (40 μM) and sodium ascorbate (2 mM) in PBS buffer pH = 7.4. (c)

6 were designed with progressively shorter aliphatic chains but otherwise a structure directly analogous to **SCNP-2a** (Figure 8a). A neutral, but very hydrophilic nanoparticle (**SCNP-7**) was also prepared.

To have a more quantitative measure of the SCNP's ability to bind hydrophobic substrates, pyrene uptake experiments were performed, where the percent of pyrene extracted from chloroform into the aqueous layer provides a direct measure of the ability of the SCNP to bind a hydrophobic substrate. As seen in Figure 8b and 8c, there is an excellent correlation between catalytic activity and the ability of the SCNP to take up pyrene. Replacing the butyl group to methyl minimally decreases the rate of the click reaction and the pyrene uptake (compare **SCNP-2a** and **SCNP-5**) suggesting that the peripheral butyl groups minimally participate in binding and catalysis. In contrast, **SCNP-6** and **SCNP-7**, show little binding and little catalysis. It is likely that these two polymeric nanoparticles are too hydrophilic to significantly bind substrate.

As seen in Figure 1, four nanoparticles, **SCNP-1a-d**, were prepared with roughly the same degree of polymerization but different **M1** to **M2**

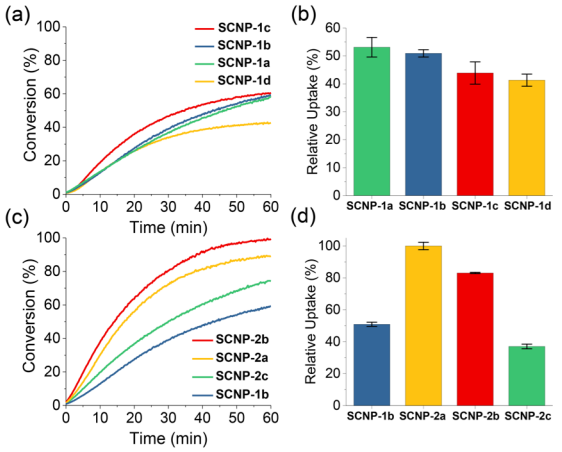

Figure 9. (a) Rate of fluorogenic CuAAC click reactions performed with **1** (20 μM), **2** (40 μM), sodium ascorbate (2 mM) and 1 μM SCNP. (b) Pyrene uptake by SCNP. (d) Fluorogenic CuAAC click reaction performed with **1** (20 μM), **2** (40 μM), sodium ascorbate (2 mM) and 1 μM **SCNP-1b**. Other SCNP run at same mass concentration. (d) Pyrene uptake by SCNP. Pyrene uptake by **SCNP-2a** was set at 100% relative uptake here and (b). The molecular weight of **SCNP-1b**, **SCNP-2a**, **SCNP-2b** and **SCNP-2c** were 76 kDa, 38 kDa, 19 kDa and 8 kDa respectively.

ratios. An increase in the **M2**:**M1** ratio increases both the crosslinking density and the number of copper complexes per SCNP. To determine the role of these two variables, the rate of the fluorogenic CuAAC click reaction was measured at 1 μM of each SCNP. Using a constant SCNP concentration means that the solution of **SCNP-1d** contained six times more copper than did **SCNP-1a**. As seen in Figure 9a, the reaction rates of all four SCNP were very similar. Despite **SCNP-1d** containing the largest amount of copper ion, it showed the slowest rate. Dye uptake experiments were also conducted and as shown in Figure 9b. The four SCNPs exhibited comparable results, each SCNP solubilizing the hydrophobic pyrene structure in water between 43-57% of that solubilized by **SCNP-2a**. The increased copper content is expected to be accompanied by a more tightly cross-linked and more polar polymer interior and this is reflected in the regular, albeit small, decrease in pyrene uptake. Overall, the results suggest that the copper content is less important than the SCNP capacity for hydrophobic binding.

The same general approach was used to determine the importance of nanoparticle size, the size decreasing along the series **SCNP-1b** < **SCNP-2a** < **SCNP-2b** < **SCNP-2c** (Figure 9c and 9d). The dye uptake experiments were performed at the same mass concentrations. SCNP size appears to matter more than copper content, although the effect both on rate and pyrene uptake is not large. The results are again consistent with the rate correlating with SCNP pyrene uptake and further suggesting that intermediate sized SCNP will give the fastest catalysts. It is possible that small polymers might not have enough flexibility to form hydrophobic pockets whereas large polymers might pack too tightly.

Enzyme-Mimetic Behavior by SCNPs as Revealed by Kinetic Analysis. Given that the combined results of the STD, 2D-NOESY, and pyrene uptake experiments, suggest that the SCNPs catalyze the CuAAC click reaction by binding the azide and alkyne in proximity to the metal catalytic site, we sought to apply enzyme kinetics to the **SCNP-2a** catalyzed CuAAC click reaction of **1** and **2**. Because the CuAAC click reaction is a two-substrate reaction that requires binding of both

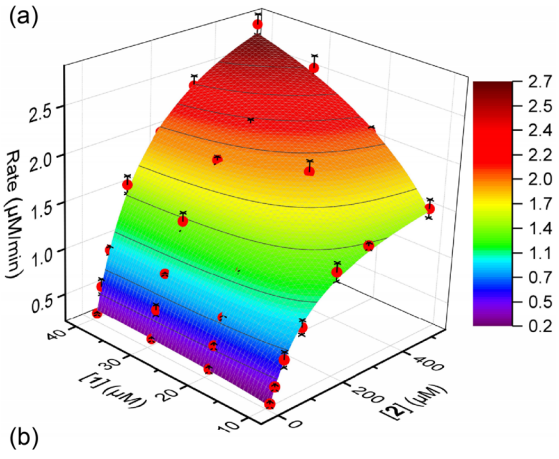

$$v = \frac{V_{max}[A][B]}{K_S^A K^{AB} + K^{AB}[A] + K^{BA}[B] + [A][B]}$$

Parameters	Value
V_{max} (μM/min)	5.0 ± 0.4
K_S^A (μM)	52 ± 32
K^{AB} (μM)	18 ± 3.6
K^{BA} (μM)	178 ± 34
R-Square	0.99

Figure 10. (a) Random-sequential two substrates enzyme kinetics equation fitting of **SCNP-2a** kinetics data. (b) Fitting equation and parameters.

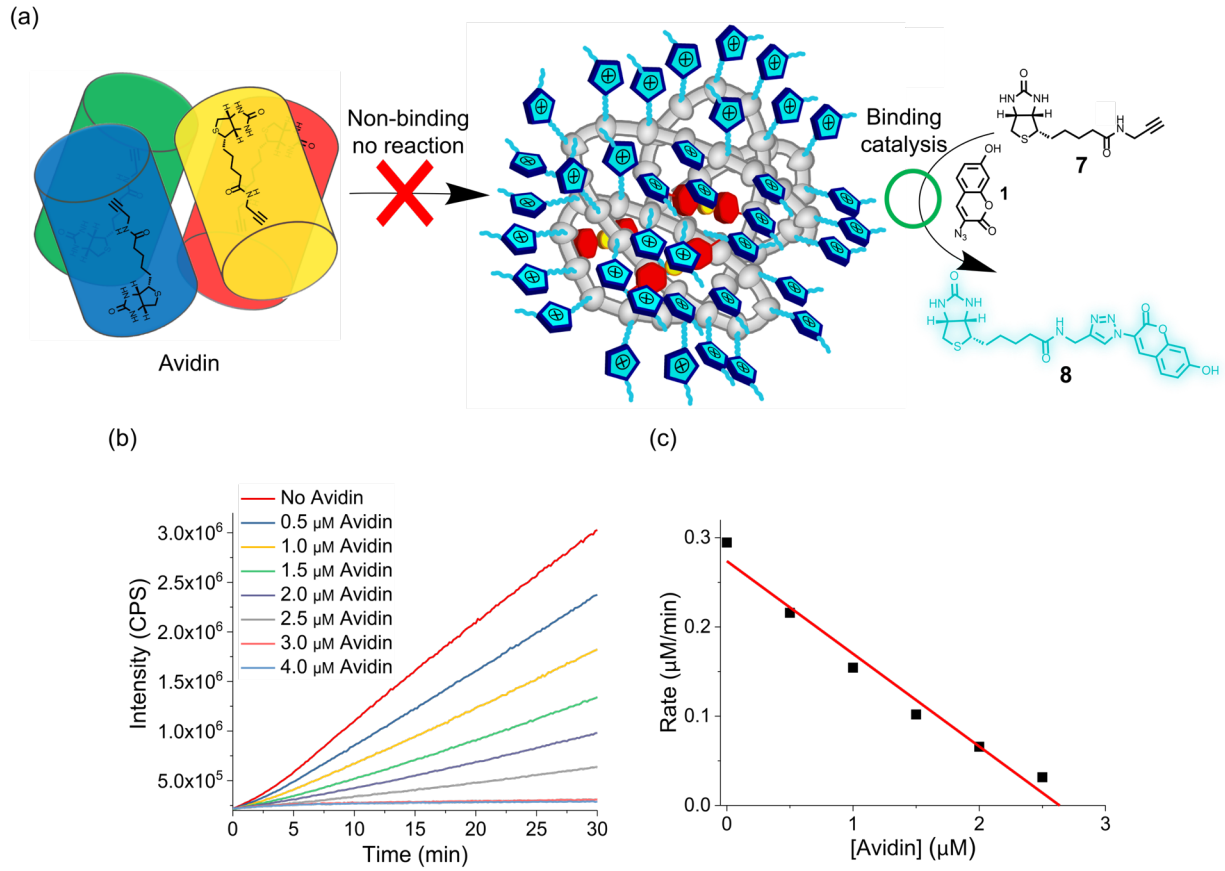

Figure 11. (a) Illustration of selective catalysis on free substrates by SCNPs. (b) Fluorogenic CuAAC click reaction on **7** (10 μM) with **SCNP-2a** (4 μM) at different avidin concentration in PBS buffer pH=7.4. The ratio of avidin to **7** was varied from 0:5 to 2:5. (c) Reaction rate over the concentration of avidin.

substrates in random sequence, the kinetics data were analyzed using the random-sequential Bi-Bi model.[18]

By varying both substrate concentrations and measuring the rate of the CuAAC click reaction between **1** and **2**, a three-dimensional rate surface was generated as shown in Figure 10. Looking along each concentration axis separately, i.e., holding one component constant and increasing the other, it can be seen that the reaction rate gradually reaches saturation, consistent with Michaelis-Menton-like kinetics. The surface in Figure 9 could be fit to the equation describing a random-sequential Bi-Bi model with the R-square as high as 0.99. Palmans, Meijer, and coworkers have reported[11] one of the few examples of Michaelis-Menten kinetics, but to our knowledge, this represents the first demonstration of two substrate enzyme kinetic behavior for an SCNP-based catalyst.

Toward The Use of SCNP in Bioapplications. We previously demonstrated that copper-containing SCNP could perform click reactions both in bacterial and mammalian cells. Here the interest was in exploring the potential use of SCNP in an additional application. As supported by the results above, substrate binding is the key step during the catalysis performed by the SCNP. If the substrate has a higher binding affinity toward another macro-molecular scaffold and is deeply buried inside a binding pocket, the reactive group on the substrate would be unreactive toward the SCNP because of the steric effect of the polymeric structure. Thus, free molecules would readily undergo the click transformation whereas bound molecules would not. Such an approach might provide a simple click-based alternative to fragment based drug discovery.[25]

To test the general principle of binding-inhibited SCNP-click, biotin and avidin was chosen because of its strong noncovalent binding, relatively buried binding site, and utility in a range of applications.[26] Each avidin molecule offers four binding sites (Figure 11). Alkyne substrate **7** was prepared with a short linker to the biotin unit, which ensures the alkyne group will be deeply buried inside the protein (Supporting Information). During the fluorogenic click reaction, the concentrations of **SCNP-2a**, **1** and **7** were kept constant, and reaction kinetics were measured with increasing concentration of avidin. Thus, the concentration of free **7** that is accessible to the nanoparticle progressively decreased with a concomitant reduction in reaction rate that is linearly correlated with the avidin concentration (Figure 11c) consistent with the experimental design.

CONCLUSION

Copper crosslinked single-chain organic nanoparticles were designed and synthesized with cationic, anionic, zwitterion, and neutral water-solubilizing groups. By using alkyne substrates with different charges and varying alkyl chain length, a structure-activity relationship was developed. In addition, the size of the polymeric nanoparticle and number of copper centers per particle were varied. The overall picture that emerges is that the rate of the copper-containing SCNP is governed primarily by the hydrophobic character of the substrate and polymer and the charge complementarity. The other factors appear to be less critical although an intermediate-sized polymer appears to have some advantages over larger and smaller SCNPs.

The structure-activity relationship combined with the STD spectroscopy, 2D-NOESY, and computational experiments strongly support the binding of both the alkyne and azide as critical for providing the enhanced rate and substrate selectivity. Indeed, the synthetic single-chain nanoparticle catalysts exhibited two-substrate enzyme kinetics behavior, making the analogy to a metalloenzyme apt. Model studies with avidin and alkyne-labeled biotin show the potential use of SCNP in

drug discovery. We are actively working on extending this system to other metal centers, and modifying the macromolecular scaffolds to afford greater rate enhancements for biolabeling both *in vitro* and *in cellulo* and the results of these efforts will be report in due course.

ASSOCIATED CONTENT

Supporting Information.

The Supporting Information is available free of charge on the ACS Publications website at DOI:

General experimental procedures and detailed synthetic procedures and characterization data for small molecules and polymers, and additional kinetic data along with details of the computational methods (PDF)

AUTHOR INFORMATION

Corresponding Author

*sczimmer@illinois.edu

ORCID

Junfeng Chen: 0000-0002-7100-0839

Yugang Bai: 0000-0002-9834-7517

Ke Li: 0000-0003-3851-7710

Edzna S. Garcia: 0000-0003-4935-4988

Steven C. Zimmerman: 0000-0002-5333-3437

Notes

The authors declare no competing financial interest.

ACKNOWLEDGMENT

This work was supported by the National Science Foundation (NSF CHE-1709718) and the Binational Science Foundation (2014116).

REFERENCES

(1) For lead references see: (a) Ilie, A.; Reetz, M. T. *Isr. J. Chem.* **2015**, *55*, 51–60. (b) Schwizer, F.; Okamoto, Y.; Heinisch, T.; Gu, Y.; Pellizzoni, M. M.; Lebrun, V.; Reuter, R.; Köhler, V.; Lewis, J. C.; Ward, T. R. *Chem. Rev.* **2018**, *118*, 142–231.

(2) Selected lead reviews: (a) Sasmal, P. K.; Streu, C. N.; Meggers, E. *Chem. Commun.* **2013**, *49*, 1581–1587. (b) Chankeshwara, S. V.; Indrigo, E.; Bradley, M. *Curr. Opin. Chem. Biol.* **2014**, *21*, 128–135. (c) Yang, M. Y.; Li, J.; Chen, P. R. *Chem. Soc. Rev.* **2014**, *43*, 6511–6526. (d) Bai, Y.; Chen, J.; Zimmerman, S. C. *Chem. Soc. Rev.* **2018**, *47*, 1811–1821. (e) Martinez–Calvo, M.; Mascarenas, J. L. *Coord. Chem. Rev.* **2018**, *359*, 57–79.

(3) (a) Gonzalez-Burgos, M.; Latorre-Sanchez, A.; Pomposo, J. A. *Chem. Soc. Rev.* **2015**, *44*, 6122–6142. (b) Altintas, O.; Barner-Kowollik, C. *Macromol. Rapid Commun.* **2016**, *37*, 29–46. (c) Mavila, S.; Eivgi, O.; Berkovich, I.; Lemcoff, N. G. *Chem. Rev.* **2016**, *116*, 878–961. (d) Rubio-Cervilla, J.; González, E.; Pomposo, J. *Nanomater.* **2017**, *7*, 341–360. (e) Pomposo J. A., ed. Single-Chain Polymer Nanoparticles: Synthesis, Characterization, Simulations, and Applications. John Wiley & Sons: 2017.

(4) (a) Bai, Y.; Feng, X.; Xing, H.; Xu, Y.; Kim, B. K.; Baig, N.; Zhou, T.; Gewirth, A. A.; Lu, Y.; Oldfield, E.; Zimmerman, S. C. *J. Am. Chem. Soc.* **2016**, *138*, 11077–11080.

(5) Huerta, E.; Genabeek, B. v.; Stals, P. J. M.; Meijer, E. W.; Palmans, A. R. A. *Macromol. Rapid Commun.* **2014**, *35*, 1320–1325.

(6) Terashima, T.; Mes, T.; De Greef, T. F. A.; Gillissen, M. A. J.; Besenius, P.; Palmans, A. R. A.; Meijer, E. W. *J. Am. Chem. Soc.* **2011**, *133*, 4742–4745.

(7) Liu, Y.; Pauloehrl, T.; Presolski, S. I.; Albertazzi, L.; Palmans, A. R. A.; Meijer, E. W. *J. Am. Chem. Soc.* **2015**, *137*, 13096–13105.

(8) Zhang, Y.; Tan, R.; Gao, M.; Hao, P.; Yin, D. *Green Chem.* **2017**, *19*, 1182–1193.

(9) Thanneeru, S.; Duay, S. S.; Jin, L.; Fu, Y.; Angeles-Boza, A. M.; He, J. *ACS Macro. Lett.* **2017**, *6*, 652–656.

(10) (a) Sanchez-Sanchez, A.; Arbe, A.; Kohlbrecher, J.; Colmenero, J.; Pomposo, J. A. *Macromol. Rapid Commun.* **2015**, *36*, 1592–1597. (b) Azuma, Y.; Terashima, T.; Sawamoto, M. *ACS Macro. Lett.* **2017**, *6*, 830–835.

(11) Huerta, E.; Stals, P. J. M.; Meijer, E. W.; Palmans, A. R. A. *Angew. Chem. Int. Ed.* **2013**, *52*, 2906–2910.

(12) (a) Artar, M.; Souren, E. R. J.; Terashima, T.; Meijer, E. W.; Palmans, A. R. A. *ACS Macro. Lett.* **2015**, *4*, 1099–1103. (b) Stals, P. J. M.; Cheng, C.-Y.; van Beek, L.; Wauters, A. C.; Palmans, A. R. A.; Han, S.; Meijer, E. W. *Chem. Sci.* **2016**, *7*, 2011–2015.

(13) (a) Wendland, M. S.; Zimmerman, S. C. *J. Am. Chem. Soc.* **1999**, *121*, 1389–1390. (b) Schultz, L. G.; Zhao, Y.; Zimmerman, S. C. *Angew. Chem. Int. Ed.* **2001**, *40*, 1962–1966. (c) Lemcoff, N. G.; Spurlin, T. A.; Gewirth, A. A.; Zimmerman, S. C.; Beil, J. B.; Elmer, S. L.; Vandeveer, H. G. *J. Am. Chem. Soc.* **2004**, *126*, 11420–11421. (d) Bai, Y.; Xing, H.; Vincil, G. A.; Lee, J.; Henderson, E. J.; Lu, Y.; Lemcoff, N. G.; Zimmerman, S. C. *Chem. Sci.* **2014**, *5*, 2862–2868.

(14) (a) Zimmerman, S. C.; Wendland, M. S.; Rakow, N. A.; Zharov, I.; Suslick, K. S. *Nature* **2002**, *418*, 399–403. (b) Zimmerman, S. C.; Quinn, J. R.; Burakowska, E.; Haag, R. *Angew. Chem. Int. Ed.* **2007**, *46*, 8164–8167. (c) Burakowska, E.; Quinn, J. R.; Zimmerman, S. C.; Haag, R. *J. Am. Chem. Soc.* **2009**, *131*, 10574–10580.

(15) (a) Bai, Y.; Xing, H.; Wu, P.; Feng, X.; Hwang, K.; Lee, J. M.; Phang, X. Y.; Lu, Y.; Zimmerman, S. C. *ACS Nano* **2015**, *9*, 10227–10236. (b) Li, Y.; Bai, Y.; Zheng, N.; Liu, Y.; Vincil, G. A.; Pedretti, B. J.; Cheng, J.; Zimmerman, S. C. *Chem. Commun.* **2016**, *52*, 3781–3784.

(16) (a) Rostovtsev, V. V.; Green, L. G.; Fokin, V. V.; Sharpless, K. B. *Angew. Chem. Int. Ed.* **2002,** *41*, 2596–2599. (b) Tornoe, C. W.; Christensen, C.; Meldal, M. *J. Org. Chem.* **2002,** *67*, 3057–3064.

(17) (a) Sivakumar, K.; Xie, F.; Cash, B. M.; Long, S.; Barnhill, H. N.; Wang, Q. *Org. Lett.* **2004**, *6*, 4603–4606. (b) Zhou, Z.; Fahrni, C. J. *J. Am. Chem. Soc.* **2004**, *126*, 8862–8863. (c) Le Droumaguet, C.; Wang, C.; Wang, Q. *Chem. Soc. Rev.* **2010**, *39*, 1233–1239.

(18) (a) Cleland, W. W. *Biochim. Biophys. Acta* **1963**, *67*, 104–137. (b) Ivanetich, K. M.; Goold, R. D. *Biochim. Biophys. Acta, Protein Struct. Mol. Enzymol.* **1989**, *998*, 7–13.

(19) (a) Diederich, F.; Dick, K. *J. Am. Chem. Soc.* **1984,** *106*, 8024–8036. (b) Denti, T. Z. M.; vanGunsteren, W. F.; Diederich, F. *J. Am. Chem. Soc.* **1996,** *118*, 6044–6051. (c) Basu Ray, G.; Chakraborty, I.; Moulik, S. P. *J. Coll. Interf. Sci.* **2006**, *294*, 248–254.

(20) Abraham, M. J.; Murtola, T.; Schulz, R.; Páll, S.; Smith, J. C.; Hess, B.; Lindahl, E. *SoftwareX* **2015**, *1*, 19–25.

(21) Choi, T.-L.; Grubbs, R. H. *Angew. Chem. Int. Ed.* **2003**, *115*, 1785–1788.

(22) (a) Van Heeswijk, W. A. R.; Eenink, M. J. D.; Feijen, J. *Synthesis* **1982**, *1982*, 744–747. (b) Thomas, G.; Zacharias, P. S. *Polyhedron* **1985**, *4*, 811–816. (c) Cerda, B. A.; Wesdemiotis, C. *J. Am. Chem. Soc.* **1995**, *117*, 9734–9739.

(23) (a) Soriano del Amo, D.; Wang, W.; Jiang, H.; Besanceney, C.; Yan, A. C.; Levy, M.; Liu, Y.; Marlow, F. L.; Wu, P. *J. Am. Chem. Soc.* **2010**, *132*, 16893–16894. (b) Besanceney-Webler, C.; Jiang, H.; Zheng, T.; Feng, L.; Soriano del Amo, D.; Wang, W.; Klivansky, L. M.; Marlow, F. L.; Liu, Y.; Wu, P. *Angew. Chem. Int. Ed.* **2011**, *50*, 8051–8056. (c) See also: Hong, V.; Presolski, S. I.; Ma, C.; Finn, M. G. *Angew. Chem. Int. Ed.* **2009**, *48*, 9879–9883.

(24) (a) Mayer, M.; Meyer, B. *Angew. Chem. Int. Ed.* **1999**, *38*, 1784–1788. (b) Mayer, M.; Meyer, B. *J. Am. Chem. Soc.* **2001**, *123*, 6108–6117.

(25) Selected lead reviews: (a) Kolb, H. C.; Sharpless, K. B. *Drug Discov. Today* **2003,** *8*, 1128–1137. (b) Lipinski, C.; Hopkins, A.

Nature **2004,** *432*, 855–861. (c) Hajduk, P. J.; Greer, J. *Nat. Rev. Drug Discov.* **2007,** *6*, 211–219.

(26) (a) Wilchek, M.; Bayer, E. A. *Method Enzym.* **1990,** *184*, 14–45. (b) DeChancie, J.; Houk, K. N. *J. Am. Chem. Soc.* **2007,** *129*, 5419–5429. (c) Laitinen, O. H.; Nordlund, H. R.; Hytonen, V. P.; Kulomaa, M. S. *Trends Biotechnol.* **2007,** *25*, 269–277.